Spectroscopic Evidence for the Two C−H-Cleaving Intermediates of *Aspergillus nidulans* Isopenicillin *N* Synthase

Esta Tamanaha,[†,⊥] Bo Zhang,[‡,⊥] Yisong Guo,[‡] Wei-chen Chang,[‡] Eric W. Barr,[†,‡] Gang Xing,[†,‡] Jennifer St. Clair,[†] Shengfa Ye,*[,§] Frank Neese,[§] J. Martin Bollinger, Jr.,*[,†,‡] and Carsten Krebs*[,†,‡]

[†]Department of Biochemistry and Molecular Biology and [‡]Department of Chemistry, The Pennsylvania State University, University Park, Pennsylvania 16802, United States

[§]Max-Planck Institute for Chemical Energy Conversion, 45470 Mülheim a. d. Ruhr, Germany

Ⓢ *Supporting Information*

ABSTRACT: The enzyme isopenicillin *N* synthase (IPNS) installs the β-lactam and thiazolidine rings of the penicillin core into the linear tripeptide L-δ-aminoadipoyl-L-Cys-D-Val (ACV) on the pathways to a number of important antibacterial drugs. A classic set of enzymological and crystallographic studies by Baldwin and co-workers established that this overall four-electron oxidation occurs by a sequence of two oxidative cyclizations, with the β-lactam ring being installed first and the thiazolidine ring second. Each phase requires cleavage of an aliphatic C−H bond of the substrate: the *pro-S*-$C_{Cys,\beta}$−H bond

for closure of the β-lactam ring, and the $C_{Val,\beta}$−H bond for installation of the thiazolidine ring. IPNS uses a mononuclear non-heme-iron(II) cofactor and dioxygen as cosubstrate to cleave these C−H bonds and direct the ring closures. Despite the intense scrutiny to which the enzyme has been subjected, the identities of the oxidized iron intermediates that cleave the C−H bonds have been addressed only computationally; no experimental insight into their geometric or electronic structures has been reported. In this work, we have employed a combination of transient-state-kinetic and spectroscopic methods, together with the specifically deuterium-labeled substrates, A[d_2-C]V and AC[d_8-V], to identify *both* C−H-cleaving intermediates. The results show that they are high-spin Fe(III)-superoxo and high-spin Fe(IV)-oxo complexes, respectively, in agreement with published mechanistic proposals derived computationally from Baldwin's founding work.
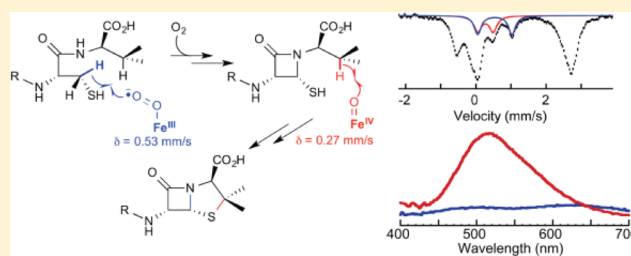
INTRODUCTION

Shortly after Sir Alexander Fleming's ingenious—albeit somewhat fortuitous—discovery of the antimicrobial activity exhibited by a secretion from a *Penicillium* mold,[1] the compound exhibiting this activity, which Fleming termed penicillin, revolutionized medicine.[2−4] The chemical moiety responsible for penicillin's antimicrobial activity is the β-lactam ring. β-Lactam antibiotics irreversibly form a covalent acyl-adduct with the catalytically essential serine residue of transpeptidase, an enzyme essential to the biosynthesis of the peptidoglycan component of the bacterial cell wall.[5] Unfortunately, extensive use of penicillin and other β-lactams for the treatment of bacterial infections has led to widespread resistance.[6] This resistance arises from β-lactamase enzymes, which hydrolyze the β-lactam ring, forming products that are innocuous to transpeptidase and the bacteria.[7] In efforts to combat resistance, other less readily hydrolyzed β-lactams, such as carbapenems, have been put into clinical practice, and inhibitors of the β-lactamases, such as clavulanic acid,[8] have been coformulated with penicillins in combination drugs (e.g., Augmentin).[9]

Early work revealed that penicillin is derived from the tripeptide δ-(L-α-aminoadipoyl)-L-cysteinyl-D-valine (ACV).[10,11] This precursor is produced by the enzyme ACV

synthetase, a nonribosomal peptide synthetase that condenses the monomeric precursors, L-α-aminoadipoate, L-cysteine, and L-valine, as it epimerizes C_α of the valine.[12−15] Conversion of ACV to isopenicillin *N* (IPN), a reaction that installs both the β-lactam and thiazolidine rings (Scheme 1), is catalyzed by the mononuclear non-heme-iron(II) [MNH-Fe(II)] enzyme, iso-penicillin *N*-synthase (IPNS).[16−19] IPN is then further processed in different ways to produce the useful β-lactam antibiotics, for example, penicillin *G* and the cephalosporins.[9,19]

IPNS belongs to the large and functionally diverse class of MNH-Fe(II) enzymes that couple the activation and four-electron reduction of O_2 to the oxidation (e.g., hydroxylation, halogenation, or desaturation) of their substrates.[20−24] Because most MNH-Fe(II) enzymes catalyze two-electron oxidations of their primary substrates, they often require a cosubstrate, which is oxidized to provide the other two electrons required for the complete reduction of O_2. The three most commonly used cosubstrates are 2-(oxo)glutarate (2OG), which is decarboxylated to CO_2 and succinate,[20,21,25] tetrahydrobiopterin, which is hydroxylated at the C4a position,[20,21,26] and NAD(P)H, which is oxidized to NAD(P)+.[20,21,27] IPNS belongs to the small but

Scheme 1. Reaction Catalyzed by IPNS[a]

ACV   IPN
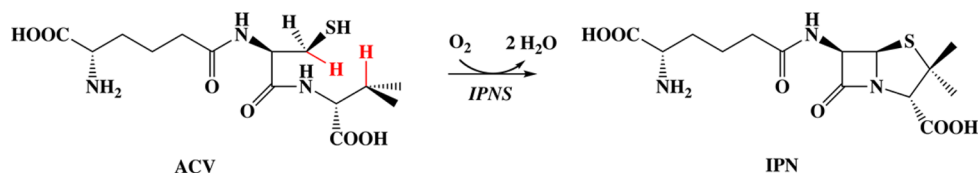
[a]Aliphatic C−H bonds cleaved during the reaction are highlighted in red.

Scheme 2. Mechanistic Hypothesis for the IPNS Reaction Arising from Prior Work of Baldwin and Co-workers[a]
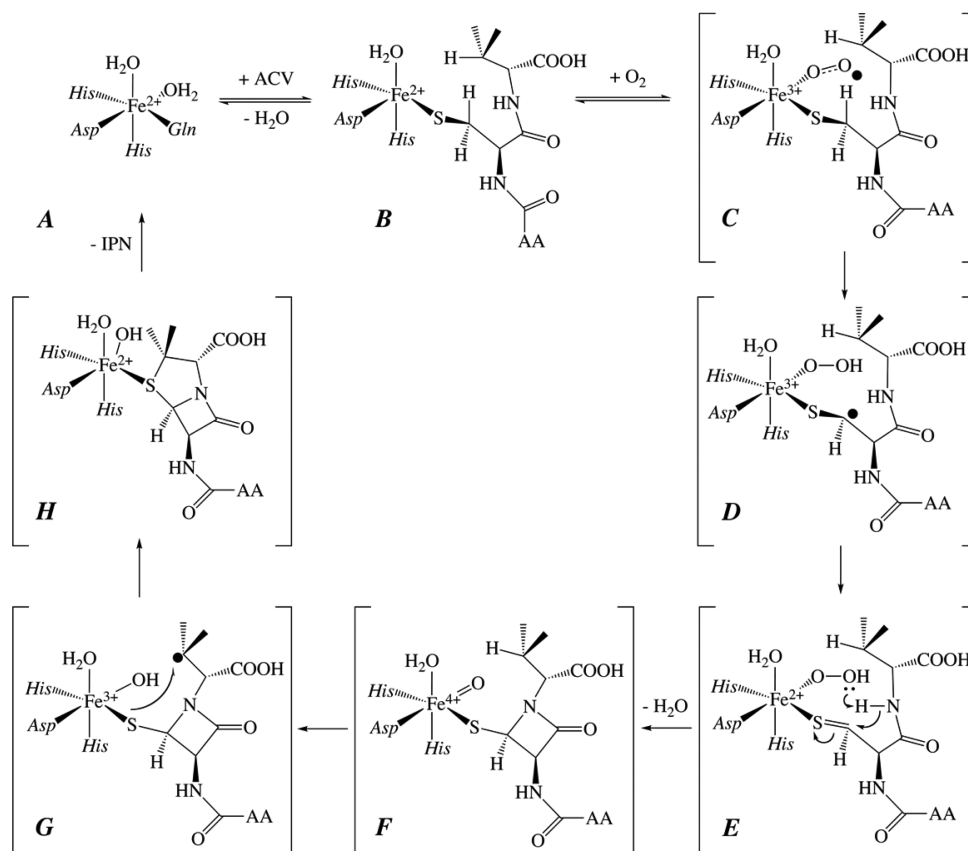
[a]AA stands for the undrawn portion of the δ-(L-α-amino)adipoyl moiety of the ACV substrate.

growing group of enzymes that extract all four electrons from their primary substrate and therefore do not require a cosubstrate.[18−21,23,28−35] Among these enzymes, IPNS is unique because it catalyzes the cleavage of *two* aliphatic C−H bonds.[18,19]

Extensive enzymological studies[18,19] and X-ray crystal structures of multiple enzyme complexes[36−39] by Baldwin and co-workers, as well as more recent computational studies,[40−43] resulted in the mechanistic hypothesis shown in Scheme 2. According to this hypothesis, the reaction proceeds in two phases, each resulting in a two-electron-oxidative cyclization. The first phase, formation of the β-lactam ring, is initiated by cleavage of the *pro-S*-$C_{Cys,\beta}$−H bond (step C → D in Scheme 2). An inner-sphere electron transfer from the resultant coordinated thioalkyl radical to the Fe(III) site yields a state with an Fe(II)-hydroperoxo complex and thioaldehyde (E). Heterolysis of the O−O bond coupled to attack of the amide on the thiocarbonyl yields an Fe(IV)-oxo (ferryl) complex with a *cis*-coordinated thiolate from the monocyclic β-lactam intermediate (F). The second phase of the reaction, which

closes the thiazolidine ring, begins with ferryl-mediated cleavage of the $C_{Val,\beta}$−H bond (F → G). Attack of the valinyl radical on the coordinated sulfur atom yields the product, isopenicillin N, with its new thioether moiety coordinated to the Fe(II) site (H).

The first evidence that formation of the β-lactam ring precedes formation of the thiazolidine ring was provided by competition experiments employing site-specifically deuterium-labeled ACV substrates.[17] A selection effect against processing of labeled substrate [a deuterium kinetic isotope effect (D-KIE) on k_{cat}/K_M] was observed for the case of $C_{Cys,\beta}$ but not $C_{Val,\beta}$ substitution, implying that $C_{Cys,\beta}$−H cleavage occurs *before* and $C_{Val,\beta}$−H cleavage *after* the first irreversible step in the mechanism. However, either individual substitution elicited a relatively large (>5) D-KIE on k_{cat}[17] and simultaneous substitution of both positions yielded an even larger effect, demonstrating that both steps are partially rate-limiting for catalytic turnover.

The founding work of Baldwin and co-workers provided compelling evidence for the sequence of ring-closure steps

shown in Scheme 2, but to our knowledge, no published experimental work has directly addressed the identities of the key C−H-bond-cleaving oxidized iron intermediates that initiate the cyclizations. Importantly, the aforementioned large D-KIEs on k_{cat} suggested that it should be possible to promote accumulation of either C−H-cleaving intermediate in a single-turnover by use of the appropriately deuterium-labeled substrate.[44−46] In this work, we have leveraged these large D-KIEs for the direct spectroscopic and computational characterization of *both* C−H-cleaving intermediates. With unlabeled ACV substrate, the $C_{Val,\beta}$−H-cleaving intermediate accumulates significantly, and the preceding $C_{Cys,\beta}$−H-cleaving complex is barely detectable. Use of the appropriate selectively deuterated substrate, δ-(L-α-aminoadipoyl)-L-3,3-[^{2}H]$_2$-cysteine-D-valine (A[d_2-C]V) or δ-(L-α-aminoadipoyl)-L-cysteine-D-2,3,4,4,4',4',4'-[^{2}H]$_8$-valine (AC[d_8-V]), promotes greater accumulation of the intermediate that cleaves that C−H bond, owing to the large D-KIE. Comparison of their spectroscopic characteristics to those of other known enzyme and inorganic complexes and analysis by density functional theory (DFT) calculations suggest that the $C_{Cys,\beta}$−H-cleaving and $C_{Val,\beta}$−H-cleaving intermediates are high-spin Fe(III)-superoxo and high-spin Fe(IV)-oxo (ferryl) complexes, respectively.

■ EXPERIMENTAL PROCEDURES

Materials and Methods. Procedures for overexpression and purification of *Aspergillus nidulans* IPNS are provided in Supporting Information. Activity of IPNS was verified by liquid chromatography/mass spectrometry (LC/MS) analysis (Figure S1). All reagents were obtained commercially (see Supporting Information), except for AC[d_8-V], which was synthesized chemically (see Supporting Information), and the identities and purities of synthetic intermediates and products were assessed by NMR spectroscopy (Figures S2−S7).

Preparation of Solutions for Stopped-Flow Absorption and Freeze−Quench Mössbauer Spectroscopies. Concentrated apo-IPNS was made anoxic by using a Schlenk line, as previously described,[47] transferred into an anoxic chamber (MBraun, Peabody, MA), and mixed in the appropriate ratio with O$_2$-free Fe(II) and ACV stock solutions to allow for formation of the reactant complex, IPNS·Fe(II)·ACV. Specific reaction conditions are given in the figure legends.

Stopped-Flow Absorption-Spectroscopic Experiments. Stopped-flow absorption (SF-abs) experiments were performed in an Applied Photophysics SX1.8MV instrument (Surrey, UK) at 5 °C with a 1 cm path length, as previously described.[47] The SF-abs unit was housed in the MBraun anoxic chamber, and data were obtained with either a photodiode array detector (PDA) or a photomultiplier tube detector (PMT). Specific reaction conditions are given in the figure legends. The IPNS·Fe(II)·ACV reactant and IPNS·Fe(II)·IPN product complexes are both nearly transparent in the visible region of the spectrum, and so transient absorption in this region arises exclusively from intermediate states. In experiments with all-protium ACV or AC[d_8-V], only the Fe(IV)-oxo contributes to this absorption at reaction times longer than ~5 ms, and so SF-abs kinetic traces monitored at 515 nm could be analyzed according to eq 2 for the concentration of an intermediate (the ferryl complex) in a sequence of two consecutive, irreversible steps (eq 1), in which the reactant (IPNS·Fe(II)·ACV), R, is converted to the Fe(IV)-oxo intermediate with an apparent first-order rate constant of k_1, the Fe(IV)-oxo intermediate decays to the product (IPNS·Fe(II)·IPN), P, with a first-order rate constant of k_2, [R]$_0$ is the concentration of the reactant complex at t = 0, and $\Delta\varepsilon_{515}$ is the difference between the molar absorption coefficients of the Fe(IV)-oxo intermediate and R (or P).

$$R \xrightarrow{k_1} \text{Fe(IV)-oxo} \xrightarrow{k_2} P \qquad (1)$$

$$\Delta A_{515}(t) = [R]_0[k_1/(k_2 - k_1)](e^{-k_1 t} - e^{-k_2 t})\Delta\varepsilon_{515} \qquad (2)$$

SF-abs experiments monitoring the absorbance changes at 515 nm in the reaction of the IPNS·Fe(II)·A[d_2-C]V complex with O$_2$ were simulated with the kinetic model shown in eq 3, which involves (i) reversible combination of O$_2$ and R, with rate constants k_1 (forward) and k_{-1} (reverse), to yield the Fe(III)-superoxo intermediate, (ii) decay of the Fe(III)-superoxo intermediate to the ferryl intermediate with a rate constant of k_2, and (iii) decay of the ferryl intermediate to P with a rate constant of k_3. The ΔA_{515}-vs-time trace from an identical experiment with unlabeled substrate was also analyzed according to the same model to obtain an estimate of the D-KIE.

$$R + O_2 \underset{k_{-1}}{\overset{k_1}{\rightleftharpoons}} \text{Fe(III)-superoxo} \xrightarrow{k_2} \text{Fe(IV)-oxo} \xrightarrow{k_3} P \qquad (3)$$
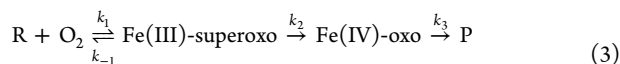
It was assumed that R and P absorb equally, so that ΔA_{515} directly reflects accumulation of the more intensely absorbing intermediates. This assumption is justified by the observation that A_{515} at t = 0 and $t \rightarrow \infty$ are equal. The ΔA_{515}-vs-time traces from reactions carried out with either unlabeled ACV or A[d_2-C]V were simulated with the software KinTek Explorer (KinTek Corporation, Snow Shoe, PA). During analysis, k_1 and k_{-1} converged to values similar to those obtained independently,[48] and k_3 was constrained to be identical to the value determined from analysis of the ΔA_{515}-vs-time traces from the reaction with unlabeled ACV according to eq 2. The error analysis for the kinetic parameters was carried using the FitSpace feature of KinTek Explorer.

Mössbauer Spectroscopy. Samples for Mössbauer spectroscopy were prepared by reacting the IPNS·Fe(II)·ACV complex with O$_2$ at 5 °C and rapidly freezing at various reaction times in cold (~125 K) 2-methylbutane, as previously described.[47] Specific conditions are given in the figure legends. Control samples of the IPNS·Fe(II) and IPNS·Fe(II)·ACV complexes were prepared in the absence of O$_2$ and hand frozen without exposure to air. Mössbauer spectra were recorded on spectrometers from Seeco (Edina, MN), as previously described[47] and were simulated by using the program WMOSS (www.wmoss.org, Seeco, Edina, MN). The simulations were carried out assuming either Lorentzian line shape (positive values of line width, Γ) or Voigt line shape (negative values of Γ). Some of the simulations are based on the commonly used spin Hamiltonian (eq 4),[49] in which the first three terms quantify the electron Zeeman effect and zero field splitting (ZFS) of the electron-spin ground state, the fourth term represents the interaction between the electric field gradient (EFG) and the nuclear quadrupole moment, the fifth term describes the magnetic hyperfine interactions of the electronic spin with the ^{57}Fe nucleus, and the last term represents the ^{57}Fe nuclear Zeeman interaction.

$$\begin{aligned}
\mathbf{H} = \ & \beta \mathbf{S}\cdot\mathbf{g}\cdot\mathbf{B} + D\left(\mathbf{S}_z^2 - \frac{S(S+1)}{3}\right) + E(\mathbf{S}_x^2 - \mathbf{S}_y^2) \\
& + \frac{\mathbf{eQV}_{zz}}{4}\left[\mathbf{I}_z^2 - \frac{I(I+1)}{3} + \frac{\eta}{3}(\mathbf{I}_x^2 - \mathbf{I}_y^2)\right] + \mathbf{S}\cdot\mathbf{A}\cdot\mathbf{I} \\
& - g_n\beta_n\mathbf{B}\cdot\mathbf{I}
\end{aligned} \qquad (4)$$

Computational Methods. Cluster models were constructed from the crystal structure of the NO adduct of IPNS (PDB 1BLZ).[38] Specifically, the active-site model contains an iron center that is coordinated by two 4-methylimidazole ligands (mimicking His214 and His270) and one acetate ligand (mimicking Asp216) in a facial arrangement, and one H$_2$O occupying the equatorial plane. Cartesian coordinates of the carbon atoms of the methyl groups, which correspond to the C_β atoms of the amino acid residues, were kept frozen during optimizations.

Geometry optimizations were performed by using the B3LYP[50,51] density functional along with the semiempirical van der Waals corrections.[52] Scalar relativistic effects were taken into account by using the zeroth-order regular approximation (ZORA)[53−55] and implemented following the model potential approximation of van Wüllen.[56] The ZORA-TZVP (Fe, O, N, and S) and ZORA-SV(P) (C and H) basis sets[57,58] were utilized. The RIJCOSX[59] approximations

were used to accelerate the calculations in combination with the auxiliary basis sets TZV/J (Fe, O, N, and S) and SV/J (remaining atoms).[60] The protein environment was crudely modeled by the conductor like screen model (COSMO)[61] with the dielectric constant set to 4.0.[62]

The Mössbauer spectroscopic parameters were computed by using the same density functional as in the geometry-optimization step. The calculation employed the CP(PPP)[63] basis set for Fe, the TZVP[64] basis set for O, N, and S, and the SV(P) basis set[65] for the remaining atoms. Isomer shifts (δ) were calculated from the electron densities at the Fe nuclei (ρ_0) employing the linear regression (eq 5):

$$\delta = \alpha \cdot (\rho_0 - C) + \beta \tag{5}$$

Here, C, α, and β are the fit parameters; their values for different combinations of the density functionals and basis sets have been reported.[66] Quadrupole splitting parameters (ΔE_Q) were obtained from electric field gradients, V_i ($i = x, y, z$; V_i are the eigenvalues of the electric field gradient tensor), employing a nuclear quadrupole moment $Q(^{57}\text{Fe}) = 0.16$ barn:[67]

$$\Delta E_Q = \frac{1}{2} e Q \cdot V_z \cdot \sqrt{1 + \frac{1}{3}\eta^2} \tag{6}$$

Here, η is the asymmetry parameter, defined as $(V_x - V_y)/V_z$. The magnetic hyperfine coupling tensor, $\mathbf{A}$, of the ^{57}Fe center was calculated by accounting for the isotropic Fermi contact term, the first-order traceless dipolar contribution, and the second-order nontraceless spin–orbit contribution. The Fermi-contact contributions for high-spin ferric and ferryl species were scaled by a factor of 1.81 according to published work.[67] Spin–orbit contributions to the hyperfine tensors were calculated as second order properties by employing the coupled perturbed (CP) Kohn–Sham theory.[68] The iron magnetic hyperfine coupling constants, A_i^{AF}, of the "genuine" antiferromagnetic state were calculated from the magnetic hyperfine coupling constants, A_i^{BS}, of the corresponding broken symmetry state by conversion into "site values" and multiplication with the spin projection coefficients, C_i:[69]

$$A_i^{AF} = C_i \frac{A_i^{BS} M_s^{BS}}{\pm S_i} \tag{7}$$

The contributions of spin orbit coupling (SOC) to ZFS were calculated by the linear response theory[70] employing the hybrid B3LYP density functional. Here, the SOC contribution to the ZFS tensor is written as

$$D_{kl}^{(SOC;M)} = f_M(S) \langle\langle h_k^{SOC}; h_l^{SOC}\rangle\rangle \tag{8}$$

In eq 8, $M = 0, \pm 1$ denotes contributions to the SOC term from excited states with $S' = S \pm 1$ ($S > 1/2$ is the total spin quantum number of the electronic state for which the ZFS tensor is computed), $f_M(S)$ is a spin-dependent prefactor ($f_0 = -1/(4S^2)$; $f_{-1} = 1/[2S(2S - 1)]$; $f_{+1} = 1/[2(S + 1)(2S + 1)]$) and $\langle\langle h_k^{SOC}; h_l^{SOC}\rangle\rangle$ is a shorthand notation for a spin–orbit linear response function. In a DFT framework, it is related to the derivatives of generalized spin-densities, as previously described.[70] The spin–spin coupling contributions to ZFSs were calculated from the equation of McWeeny and Mizuno,[71]

$$D_{kl}^{SS} = \frac{g_e^2}{4} \frac{\alpha^2}{S(2S-1)} \sum_{\mu\nu} \sum_{\kappa\tau} \{P_{\mu\nu}^{\alpha-\beta} P_{\kappa\tau}^{\alpha-\beta} - P_{\mu\kappa}^{\alpha-\beta} P_{\nu\tau}^{\alpha-\beta}\} \langle\mu\nu|r_{12}^{-5}$$
$$\{3r_{12,k}r_{12,l} - \delta_{kl}r_{12}^2\}|\kappa\tau\rangle \tag{9}$$

in which the spin density matrix, $\mathbf{P}^{\alpha-\beta}$, was obtained on the basis of the spin-unrestricted natural orbital (UNO) determinant.[72] All computations in this work were carried out with the ORCA program package.[73]

■ RESULTS

SF-abs Evidence for Accumulation of an Intermediate during the Reaction of the IPNS·Fe(II)·ACV Complex with O₂. Time-dependent absorption spectra obtained after

mixing of the IPNS·Fe(II)·ACV complex with O_2-saturated buffer at 5 °C under single-turnover conditions (with ACV limiting) exhibit transient absorption in the visible region reflecting the accumulation of an intermediate (Figure S8A). The corresponding spectra from the control experiment in which O_2 was omitted (Figure S8B) do not change with time, thus confirming that the spectral changes arise from the reaction of IPNS·Fe(II)·ACV with O_2. Subtracting the spectrum of the O_2-free control from the spectra of the reaction removes contributions from the protein and possible contaminants (Figure 1A). The difference spectra reveal that
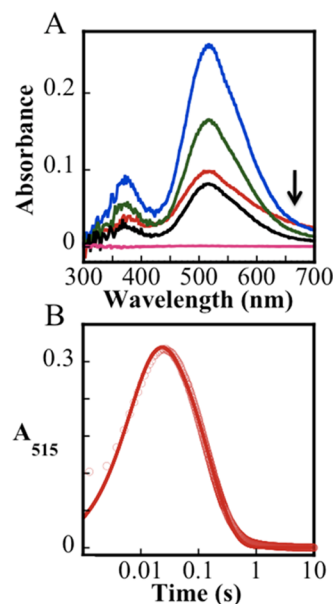

Figure 1. Stopped-flow absorption data from the reaction of the IPNS·Fe(II)·ACV complex with O_2. (A) Difference spectra generated by subtracting from experimental spectra acquired 0.002 s (red), 0.020 s (blue), 0.10 s (green), 0.20 s (black), and 2.0 s (pink) after mixing of a solution of the IPNS·Fe(II)·ACV complex (1.5 mM IPNS, 1.5 mM Fe(II), 0.5 mM ACV in 100 mM MOPS, pH 7.2) with an equal volume of oxygenated buffer (100% O_2 at 5 °C, estimated to have 1.8 mM O_2[112]) the corresponding spectra from a matched control experiment lacking O_2. (B) ΔA_{515} kinetic trace from the experiment in panel A (red circles). The red line is a fit with the parameters quoted in the text.

the intermediate exhibits absorption bands centered at ~360 and ~515 nm. The ΔA_{515}-vs-time trace from this reaction (Figure 1B, red open circles) reveals that the intermediate accumulates maximally at ~25 ms and decays completely by ~1 s. The trace can be analyzed according to a kinetic model involving two irreversible, consecutive reactions with apparent first-order rate constants of $k_1 = 125$ s^{-1} and $k_2 = 7$ s^{-1} (red line in Figure 1B).[74] The data in Figure 1A also provide a first hint of the accumulation of a preceding intermediate, as comparison of the 0.002 s spectrum (Figure 1A, red trace) to the later spectra reveals a low-energy shoulder at very early reaction times (arrow). Accumulation of this precursor is confirmed by additional experiments described below.

Mössbauer Spectroscopic Evidence for an Fe(IV) Intermediate. Freeze–quench Mössbauer spectroscopic (FQ-Möss) experiments afforded insight into the nature of the intermediate detected in the SF-abs experiments.[49,75,76] The 4.2-K/zero-field spectrum of the reactant complex (Figure 2, top, vertical bars) can be simulated as a weighted superposition
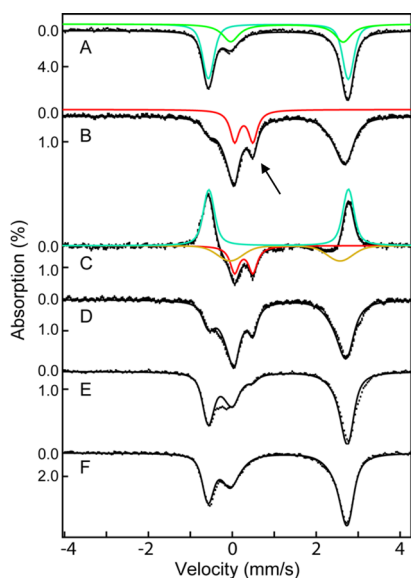
Figure 2. Mössbauer spectra (4.2-K/zero-field) of samples prepared by reacting the IPNS·Fe(II)·ACV complex with O_2 at 5 °C and freeze quenching after the indicated reaction times. Spectrum of an O_2-free solution of the reactant IPNS·Fe(II)·ACV complex (1.8 mM IPNS, 1.8 mM Fe(II) and 20 mM ACV in 100 mM MOPS, 10% glycerol, pH 8.3) (A), and spectra of samples prepared by mixing the reactant complex (above) with an oxygen-saturated solution of buffer (at 5 °C, ~1.8 mM O_2) in a 1:2 (v/v) ratio and freeze-quenching after reaction times of 0.020 s (B), 0.12 s (D), 0.45 s (E), and 90 s (F) are shown as vertical bars. Spectrum C is the difference spectrum B − A. The solid green, turquoise, gold, and red lines are simulated quadrupole doublets matching the spectra of the IPNS·Fe(II), IPNS·Fe(II)·ACV, and IPNS·Fe(II)·IPN complexes and Fe(IV)-oxo intermediate, respectively; the parameters used to generate them are given in the text. The arrow marks the high-energy line of the spectrum of the Fe(IV)-oxo intermediate.

of a sharp and well-defined quadrupole doublet (δ_1 = 1.10 mm/s, $|\Delta E_{Q,1}|$ = 3.35 mm/s, and Γ = −0.25 mm/s, 65% of total intensity, turquoise line) and a broad quadrupole doublet (δ_2 = 1.30 mm/s, $|\Delta E_{Q,2}|$ = 2.68 mm/s, and Γ = −0.61 mm/s, 35% of total intensity, green line). The parameters are typical for high-spin Fe(II) sites and are virtually identical to those of the ternary IPNS·Fe(II)·ACV complex (δ_1 = 1.11 mm/s and $\Delta E_{Q,1}$ = 3.43 mm/s) and the binary IPNS·Fe(II) complex (δ_2 = 1.30 mm/s and $\Delta E_{Q,2}$ = 2.70 mm/s), respectively, reported for *Cephalosporium acremonium* IPNS.[77] Consistent with previous results, only ~70% of the added Fe(II) yields the ternary IPNS·Fe(II)·ACV complex, as determined from analysis of the Mössbauer spectra.[77] The unusual breadth of the quadrupole doublet assigned to the binary IPNS·Fe(II) complex suggests heterogeneity in this state.

The 4.2-K/zero-field Mössbauer spectra of samples prepared by reacting the IPNS·Fe(II)·ACV complex with O_2 at 5 °C for 0.020, 0.12, 0.45, or 90 s (Figure 2, vertical bars) before freeze-quenching reveal changes associated with the reaction. Most notably, a peak at approximately +0.5 mm/s (Figure 2, arrow) reaches maximum intensity in the spectrum of the 0.020 s sample and then decays. This peak is the high-energy line of a quadrupole doublet associated with a reaction intermediate. Its parameters can be determined by subtracting the spectrum of the reactant control sample from that of the 0.020 s sample, which allows the position of the low-energy line of the quadrupole doublet to be discerned. Analysis of this difference

spectrum reveals that the reaction results in conversion of 55% of the reactant IPNS·Fe(II)·ACV complex (simulated with the above parameters, turquoise line pointing upward) to 28% of the new quadrupole doublet with parameters (δ = 0.27 mm/s, $|\Delta E_Q|$ = 0.44 mm/s, and Γ = 0.26 mm/s, red line in Figure 2) similar to those of high-spin Fe(IV)-oxo complexes in other MNH-Fe(II) enzymes in addition to 27% of a second new, broad quadrupole doublet with parameters (δ = 1.27 mm/s, $|\Delta E_Q|$ = 2.62 mm/s, and Γ = −0.75 mm/s, 27%, gold line in Figure 2) characteristic of high-spin Fe(II) complexes.[24] Mössbauer spectra collected in strong externally applied fields (Figure S9) confirm that, like the other known ferryl complexes in these enzymes, the IPNS Fe(IV) intermediate has an S = 2 ground state. The high-field spectra further reveal that the IPNS complex exhibits more pronounced anisotropy in the xy plane than the other high-spin ferryl intermediates (see Table 1

Table 1. Key Structural Parameters and Comparison of Calculated and Experimental Spin-Hamiltonian Parameters of the Fe(IV)-oxo Intermediate

parameter	I	II	III	exptl
Fe−O$_{oxo}$ (Å)	1.645	1.642	1.637	
Fe−S (Å)	2.327	2.706	2.705	
Fe−O$_{H2O/OH}$ (Å)	2.235	1.831	1.843	
D (cm^{-1})	3.5	3.1	3.1	10
E/D	0.19	0.31	0.28	0.09
δ (mm/s)	0.25	0.12	0.15	0.27
ΔE_Q (mm/s)	−0.93	−0.69	+0.30	−0.44
η	0.2	0.4	0.7	1.5
A (MHz)	−21.9	−16.1	−17.3	−23.7
	−15.5	−8.8	−11.3	−17.8
	−32.4	−25.8	−27.3	−41.3

and Supporting Information for analysis of these spectra). The third, broad quadrupole doublet required to account for the difference spectrum is attributable to one or more Fe(II) complex(es) formed during the reaction, likely including the IPNS·Fe(II)·IPN product complex.

The entire set of time-dependent spectra can be analyzed as weighted superpositions of the above four quadrupole doublets, with the contribution of the IPNS·Fe(II) complex fixed at the value determined from the spectrum of the reactant control sample (an assumption based on observations for other MNH-Fe(II) enzymes that the substrate-free forms react sluggishly with O_2).[78] The features of the Fe(IV)-oxo complex account for 28%, 21%, 5%, and <2% of the spectra of the 0.020 s, 0.12 s, 0.45 s, and 90 s samples, respectively. The quantities of the four species are compiled in Table S1.

Comparison of the time-dependencies of ΔA_{515} and the relative area of the Fe(IV)-associated quadrupole doublet from SF-abs and FQ-Mössbauer experiments carried out under nearly identical reaction conditions confirms that the absorption bands at 360 and 515 nm are associated with the Fe(IV)-oxo complex (Figures S10 and S11). Under the assumption that the reactant IPNS·Fe(II)·ACV complex does not absorb in this spectral region, this comparison affords an estimate of the molar absorptivity of the Fe(IV) species at 515 nm as 2.7 mM^{-1} cm^{-1}.

SF-abs Evidence That the Fe(IV) Complex Is the C$_{Val,\beta}$−H-Cleaving Intermediate. The assignment of the absorbing intermediate on the basis of its Mössbauer parameters as a high-spin Fe(IV) complex suggests that it could be the C$_{Val,\beta}$−

H-cleaving complex, F, in Scheme 2. We therefore tested for a D-KIE on its decay in the presence of AC[d_8-V].[78−82] The ΔA_{515}-vs-time traces from matched experiments with natural-abundance ACV (Figure 3, black trace) or the valine-labeled
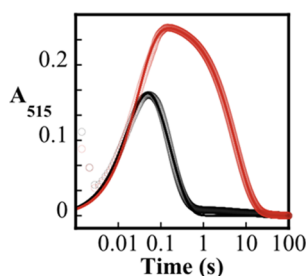

Figure 3. ΔA_{515} kinetic traces acquired after mixing of an air-saturated buffer solution (100 mM MOPS pH 7.2; 0.3 mM O_2) with an equal volume of a solution containing 3.0 mM IPNS, 3.0 mM Fe(II), 20.0 mM TCEP, and either 20.0 mM ACV (black solid circles) or 20.0 mM AC[d_8-V] (red solid circles) at 5 °C. The solid lines are simulations with parameters quoted in the text.

substrate (AC[d_8-V], with >98% ^{2}H at the target position; red trace) reveal a very large effect on decay of the Fe(IV) intermediate with no effect on ferryl formation. Analysis of the traces according to eq 2 yields an apparent first-order rate constant of formation (k_1) of ~40 s^{-1} and decay rate constants (k_2) of 7.1 and 0.2 s^{-1} for the reactions with unlabeled ACV and AC[d_8-V], respectively, from which a D-KIE of at least 30 is calculated (the true, intrinsic D-KIE may be larger if the presence of deuterium results in failed events[44]). This large D-KIE confirms that the detected Fe(IV) complex cleaves the $C_{Val,\beta}$−H bond and provides further confirmation that it is a ferryl complex.

SF-abs Evidence for Accumulation of the $C_{Cys,\beta}$−H-Cleaving Intermediate. Although the data from experiments with unlabeled ACV and AC[d_8-V] provide clear evidence for accumulation of the $C_{Val,\beta}$−H-cleaving Fe(IV) complex, there is only a hint of the possible accumulation of any preceding complex, as in the initial Fe(II)−O_2 adduct proposed in Scheme 2 to cleave the $C_{Cys,\beta}$−H bond on the pathway to the Fe(IV)-oxo complex. Therefore, the $C_{Cys,\beta}$-deuterated substrate (A[d_2-C]V) was used as a mechanistic probe, with the expectation that it would enhance accumulation of the $C_{Cys,\beta}$−H-cleaving complex.[44−46] Time-dependent spectra from SF-abs experiments monitoring the reaction of the IPNS·Fe(II)·A[d_2-C]V complex with O_2 at 5 °C (Figure S12) provide evidence for the anticipated precursor to the ferryl complex. Subtracting spectra from the control experiment lacking O_2 to cancel contributions from the protein and contaminants (Figure 4A) yields difference spectra that are markedly different at very early reaction times (red and purple traces) but then evolve at longer reaction times to the signature of the Fe(IV)-oxo complex (green and black traces). The spectrum at 0.002 s (red trace) deviates markedly from that of the Fe(IV)-oxo complex, exhibiting broad absorption maxima at ~500 and ~630 nm. The enhancement of these features by the Cys-labeled substrate implies that they are most likely associated with the $C_{Cys,\beta}$−H-cleaving complex. The difference spectrum at 0.020 s (blue trace) can be rationalized as a superposition of the spectra of the Fe(IV)-oxo intermediate and its $C_{Cys,\beta}$−H-cleaving precursor, suggesting that, at this reaction time, both intermediates have accumulated. The qualitative
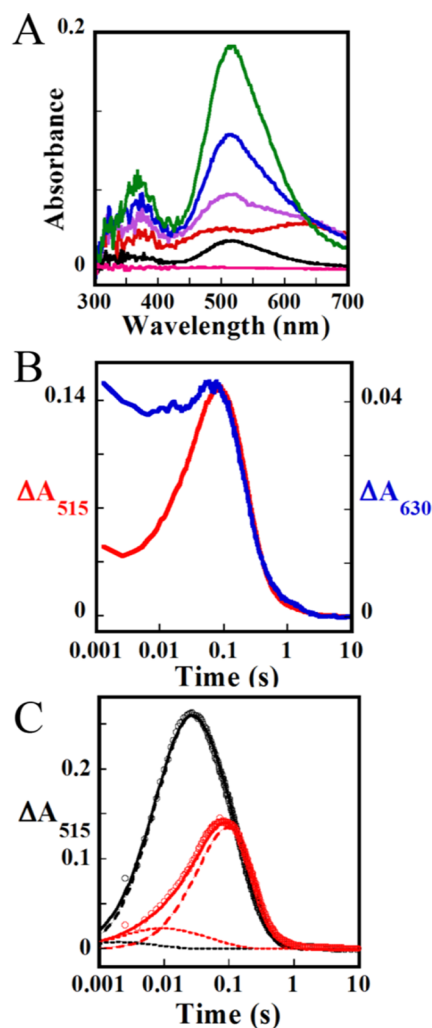

Figure 4. SF-abs data from the reaction of the IPNS·Fe(II)·A[d_2-C]V complex with O_2. (A) Difference spectra generated by subtracting from experimental spectra acquired 0.002 s (red), 0.007 s (purple), 0.020 s (blue), 0.10 s (green), 0.50 s (black), and 2.0 s (pink) after mixing of a solution containing the IPNS·Fe(II)·A[d_2-C]V complex (1.5 mM IPNS, 1.5 mM Fe(II), 0.5 mM ACV in 100 mM MOPS, pH 7.2) with an equal volume of an oxygenated buffer solution (100% O_2 at 5 °C, estimated to have 1.8 mM O_2) the corresponding spectra from a matched control experiment lacking O_2. (B) Comparison of the ΔA_{515} (red) and ΔA_{630} (blue) kinetic traces from the reaction with A[d_2-C]V. (C) Comparison of the ΔA_{515} kinetic trace from A (red circles) to that of an identical experiment carried out with unlabeled ACV (black circles). The solid lines are simulations of the traces according to the kinetic model of eq 3 and parameters k_1 = 153 mM^{-1}s^{-1}, k_{-1} = 15 s^{-1}, k_2 = 973 s^{-1} (ACV, black), k_2 = 40 s^{-1} (A[d_2-C]V, red), k_3 = 7.1 s^{-1}, with values of $\Delta \varepsilon_{515}$ of 0.67 mM^{-1}cm^{-1} and 2.7 mM^{-1}cm^{-1} for the Fe(III)-superoxo and Fe(IV)-oxo intermediates, respectively. The individual contributions from the Fe(III)-superoxo and Fe(IV)-oxo intermediates are shown as dotted and dashed lines, respectively.

similarity of the 0.020 s difference spectrum from the reaction with A[d_2-C]V (blue trace) to the 0.002 s difference spectrum from the reaction with unlabeled ACV (Figure 1A, red line) implies that the same precursor to the ferryl complex also accumulates with the unlabeled substrate. At longer times in the reaction with A[d_2-C]V, features of the ferryl intermediate come to dominate the spectrum, as in the reaction with unlabeled ACV. A comparison of scaled kinetic traces at 515

and 630 nm from the reaction with the cysteine-labeled substrate (Figure 4B) starkly illustrates the accumulation of the 630 nm-absorbing species in advance of the Fe(IV)-oxo complex.

Comparison of the ΔA_{515}-vs-time traces from the reaction of the IPNS·Fe(II)·A[d_2-C]V complex with O_2 (Figure 4C, red open circles) and the corresponding reaction with unlabeled ACV (Figure 4C, black open circles) provides additional evidence for the proposed sequence of intermediates. Because ΔA_{515} is dominated by the intense absorption from the Fe(IV)-oxo complex, the traces largely reflect formation and decay of this intermediate. The retardation of ferryl formation upon use of A[d_2-C]V reflected in this trace provides direct evidence that $C_{Cys,\beta}$–H-cleavage precedes ferryl formation (and thus also $C_{Val,\beta}$–H cleavage) and that the former process exhibits a significant D-KIE.

The simplest explanation for the enhanced accumulation of the 630 nm-absorbing complex with A[d_2-C]V is that it is the species that cleaves the $C_{Cys,\beta}$–H bond. According to this interpretation, protium is abstracted sufficiently rapidly that the responsible intermediate barely accumulates, but the D-KIE is sufficiently large to permit considerably more accumulation of this intermediate species. Analysis of ΔA_{515}-vs-time traces according to the model in eq 3 afforded estimates of decay rate constants for the Fe(III)-superoxo complex of (970 ± 240) s^{-1} and (40 ± 3) s^{-1} for the reactions with unlabeled ACV and A[d_2-C]V, respectively, from which the D-KIE for $C_{Cys,\beta}$–H cleavage can be estimated to be 17−33. We also considered the alternative possibility that (i) the slower cleavage of the $C_{Cys,\beta}$–D bond results in uncoupling of the reaction and allows formation of an off-pathway complex to compete more effectively with $C_{Cys,\beta}$–H cleavage and (ii) the transient absorption at ~630 nm is largely contributed by this off pathway complex. Analysis of the ΔA_{515}-vs-time trace according to this model (Figure S13) reveals that uncoupling due to the deuterium substitution is, at most, only modest (~20%). While this analysis alone does not provide definitive evidence that the long-wavelength absorption features are associated with the on-pathway ($C_{Cys,\beta}$–H-cleaving) intermediate, the corresponding FQ-Mössbauer experiments (see below) reveal accumulation of a new intermediate to levels that exceed the maximum flux through the hypothetical uncoupling pathway that could be accommodated by the SF-abs data. Consistent with the interpretation that the long-wavelength features arise from the $C_{Cys,\beta}$–H-cleaving complex, it has been reported that A[S-d_1-C]V is successfully processed to the all-protium IPN product (i.e., the reaction proceeds with abstraction of the *pro*-S-deuterium), although the product of this reaction was not quantified and the formation of alternative products was not explored.[83]

Mössbauer Spectroscopic Evidence That the $C_{Cys,\beta}$–H-Cleaving Intermediate Is a Fe(III)-superoxo Complex. The $C_{Cys,\beta}$–H-cleaving intermediate was further characterized by FQ Mössbauer spectroscopic experiments with A[d_2-C]V. Time-dependent, 4.2-K/zero-field Mössbauer spectra of samples prepared by reacting the IPNS·Fe(II)·A[d_2-C]V complex with O_2 at 5 °C (Figure 5, vertical bars) reveal the presence of a new absorption peak at ~1 mm/s (see arrow) that develops to its maximum intensity by the first accessible reaction time and decays in less than a second. Because this peak develops to a much greater extent with the Cys-deuterated substrate, it is attributable to the 610 nm-absorbing, $C_{Cys,\beta}$–H-cleaving intermediate. The peak is the high-energy line of a
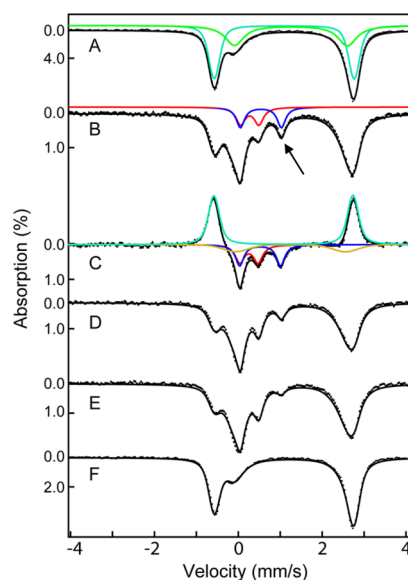

Figure 5. Time-dependent 4.2-K/zero-field Mössbauer spectra from the reaction of the IPNS·Fe(II)·A[d_2-C]V complex with O_2. Spectrum of the reactant complex (4.5 mM IPNS, 3.6 mM Fe(II), and 20 mM A[d_2-C]V in 100 mM MOPS, 10% glycerol at pH 7.2) (A) and spectra of samples prepared by mixing the reactant complex (above) with an oxygen-saturated solution of buffer (at 5 °C, ~1.8 mM O_2) in a 1:2 (v/v) ratio and freeze-quenching after reaction times of 0.010 s (B), 0.050 s (D), 0.13 s (E), or 130 s (F) are shown as vertical bars. Spectrum C is the difference spectrum B − A. The solid green, turquoise, gold, red, and blue lines are simulations of the quadrupole doublet spectra of the IPNS·Fe(II), IPNS·Fe(II)·ACV, and IPNS·Fe(II)·IPN complexes and the Fe(IV)-oxo and Fe(III)-superoxo intermediates, respectively, using parameters given in the text. The arrow marks the high-energy line of the spectrum of the Fe(III)-superoxo intermediate.

quadrupole doublet. Although the low-energy line is not resolved, its position could be determined by two independent approaches.

First, initial subtraction of the spectrum of the reactant control sample gave a difference spectrum that could be analyzed as a superposition of four quadrupole doublets. The parameters of the three quadrupole doublets representing the IPNS·Fe(II)·A[d_2-C]V reactant complex (turquoise line), the Fe(IV)-oxo intermediate (red line), and the Fe(II)-product complex (gold line) were set to the values determined by the analysis of the Mössbauer spectra with unlabeled ACV substrate (see above), while the parameters of the quadrupole doublet associated with $C_{Cys,\beta}$–H-cleaving intermediate were allowed to vary. This analysis returned parameters for the $C_{Cys,\beta}$–H-cleaving intermediate (δ = 0.53 mm/s, $|\Delta E_Q|$ = 1.02 mm/s, and Γ = 0.29 mm/s; blue line) typical of high-spin Fe(III) complexes with N/O-coordination.[49] The fact that the intermediate gives rise to a quadrupole doublet in the absence of applied magnetic field suggests that it has an integer-electron-spin ground state, consistent with expectations and precedent for an Fe(III)-superoxo complex, in which antiferromagnetic (AF) or ferromagnetic (F) exchange coupling between the high-spin Fe(III) (S_{Fe} = 5/2) and superoxide radical (S_{SO} = 1/2) would yield an S = 2 or S = 3 total-spin state, respectively.[49,76] The time-dependent spectra were analyzed as the superpositions of the five quadrupole doublets representing the unreactive IPNS·Fe(II) complex, the IPNS·Fe(II)·A[d_2-C]V reactant complex, the IPNS·Fe(II)·IPN product complex, and the Fe(IV)-oxo- and Fe(III)-superoxo-

containing intermediate states (black solid lines in Figure 5; see Table S2 for all parameters). Consistent with the SF-abs data, accumulation of the Fe(III)-superoxo intermediate precedes accumulation of the Fe(IV)-oxo intermediate. The complexes contribute 14%, 9%, and ~4% [Fe(III)-superoxo] and 12%, 21%, and 20% [Fe(IV)-oxo] of the total absorption area at reaction times of 0.010, 0.050, and 0.13 s, respectively.
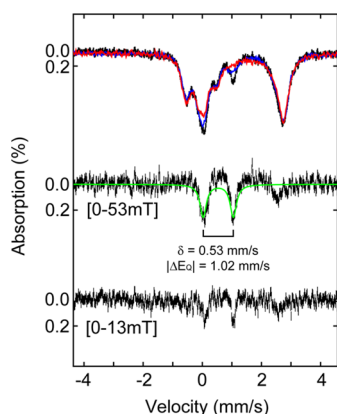

Figure 6. Mössbauer spectra (4.2-K/variable-field) of a sample prepared by mixing a solution of the reactant complex (4.5 mM IPNS, 3.6 mM Fe(II), and 20 mM A[d_2-C]V in 100 mM MOPS, 10% glycerol at pH 7.2) with an oxygen-saturated solution of buffer (at 5 °C, ~1.8 mM O$_2$) in a 1:2 (v/v) ratio and freeze-quenching after a reaction time of 0.010 s. (top) The experimental spectrum collected in zero magnetic field is shown as black vertical bars. The solid blue and red lines are the experimental spectra recorded in external magnetic fields of 13 and 53 mT, respectively. (middle) The (0 − 53) mT difference spectrum is shown as vertical bars. The green line is a theoretical simulation using parameters quoted in the main text. (bottom) The experimental (0 − 13 mT) difference spectrum is shown as vertical bars.

Second, the Mössbauer parameters of the C$_{Cys,\beta}$−H-cleaving intermediate were independently determined from spectra of the 0.010 s sample recorded in variable, weak external magnetic fields (Figure 6). Comparison of spectra recorded in zero-field and in weak applied fields (13 or 53 mT) reveals that the spectral features of the Fe(II)-containing complexes and the Fe(IV) intermediate are not (or are only slightly) broadened by the weak applied field. In contrast, the quadrupole doublet associated with the C$_{Cys,\beta}$−H-cleaving intermediate exhibits noticeable broadening in the 13 mT spectrum (blue line) and is broadened beyond recognition in the 53 mT spectrum (red line). The field-dependent broadening of the Mössbauer features of the C$_{Cys,\beta}$−H-cleaving intermediate can be visualized more clearly in the [0 mT − 53 mT] and [0 mT − 13 mT] difference spectra, in which the downward-pointing doublet represents the spectral features associated with this intermediate in zero-field. (The spectrum of the intermediate with weak applied fields cannot be readily discerned in the difference spectra, because the intermediate contributes only a modest fraction of the overall absorption and its spectrum is broad with an applied field.) Analysis of the difference spectra gives δ = 0.53 mm/s and $|\Delta E_Q|$ = 1.02 mm/s (green line), identical to the parameters determined by analysis of the 0.010 s spectrum after removal of the contributions of Fe(II) complexes. The observed broadening of the features of the Fe(III)-superoxo complex in weak applied fields gives insight into its electronic structure. The axial ZFS parameter (D) of the S = 2 or S = 3

total-spin state depends primarily on the corresponding parameter of the S = 5/2 Fe site (D_{Fe}) and is scaled by spin-projection coefficients D_{Fe} = 4/3 (S = 2) or D_{Fe} = 2/3 (S = 3).[84] Because the values of the dominating component, D_{Fe}, are typically small for high-spin Fe(III) complexes, the resulting D of the exchange-coupled system is also expected to be rather small. Consequently, the spin expectation value, $\langle S \rangle$, rises steeply with applied field, resulting in the significant internal fields that are responsible for the observed magnetic broadening even with weak applied fields.

Spectra of the 0.010 s sample were also acquired in externally applied magnetic fields of 2 and 4 T (Figure S14). Owing to the modest accumulation of the C$_{Cys,\beta}$−H-cleaving intermediate (14%) and the fact that its spectrum splits in an applied field, the outer lines associated with the intermediate could be assigned only tentatively. From the splitting of the outer lines, the magnitude of the **A**-tensor (assumed for simplicity to be isotropic) could be estimated. Analysis assuming an S = 2 electron ground state yields $A_{iso,S=2} \approx -26.2$ MHz with respect to the total spin, which corresponds to an intrinsic ^{57}Fe hyperfine coupling of $A_{iso,^{57}Fe} \approx -22.4$ MHz, using the standard spin projection method, $A_{iso,S=2} = (7/6)A_{iso,^{57}Fe}$.[84] Likewise, analysis assuming S = 3 for the total spin ground state yields $A_{iso,S=3} \approx -17.9$ MHz and $A_{iso,^{57}Fe} \approx -21.5$ MHz, using $A_{iso,S=3} = (5/6)A_{iso,^{57}Fe}$. Both $A_{iso,^{57}Fe}$ values are smaller than typical values for N/O-coordinated high-spin Fe(III) (approximately −30 MHz),[49] but similar values were reported previously for an inorganic Fe(III)-superoxo complex.[85,113] Although the intrinsic value of $A^{57}Fe$ determined for S = 2 is somewhat more typical, the available data do not allow unambiguous assignment of the spin multiplicity of the ground state. Nevertheless, the Mössbauer data provide strong evidence supporting the formulation of the C$_{Cys,\beta}$−H-cleaving intermediate as a Fe(III)-superoxo complex with an S = 2 or S = 3 total-electron-spin ground state.

Evaluation of the Intermediates by Density Functional Theory (DFT) Calculations. To evaluate the consistency of the structures assigned to the intermediates with their experimentally observed spectroscopic characteristics, we employed DFT calculations on model structures. For the Fe(IV) complex, three models were considered. Model I (Figure 7A) represents intermediate F in the proposed
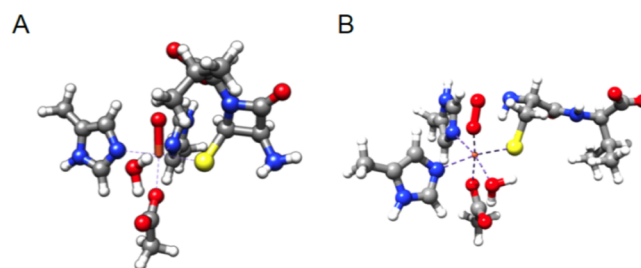

Figure 7. Optimized geometric structures of model I of the Fe(IV)-oxo intermediate (left) and model VI of the Fe(III)-superoxo intermediate (right).

mechanism (Scheme 2), with a closed β-lactam ring. Model II (Figure S15) is based on a proposal advanced in two recent computational studies. It was proposed that, to assist in O−O bond cleavage, the Fe-bound water ligand, rather than the valine N−H bond (step E → F in Scheme 2), may function as a proton donor, thereby leading to formation of a

HO−Fe(IV)=O species prior to closure of the β-lactam ring.[41,42] Finally, model III has an OH ligand coordinated to the ferryl center with a closed β-lactam ring (Figure S15). The optimized structures for models I and II are in good agreement with those reported by Lundberg et al.[41] These three models all feature a compressed octahedral coordination geometry due to the covalent Fe(IV)-oxo interaction as evidenced by the short Fe−O_{oxo} bond distances of ∼1.64 Å (Table 1). The most significant geometric difference among them is that the Fe−O_{OH} bonds in models II and III are much shorter than the corresponding Fe−O_{H_2O} bond in I, reflecting the different Lewis basicity of OH^- relative to H_2O. Moreover, models II and III have significantly longer Fe−S bonds than model I.

Of the spin-Hamiltonian parameters that can be calculated, isomer shifts typically have the greatest accuracy, with uncertainties of less than 0.1 mm/s.[63,66] Of the three models interrogated, only model I yields a computed isomer shift that agrees with the experimental value to within this established accuracy,[66] whereas the values computed for models II and III diverge from the experimental value by much more than 0.1 mm/s. Models II and III can thus be ruled out as accurate representations of the Fe(IV)-oxo intermediate. The significantly diminished isomer shifts computed for models II and III likely arise from the short Fe−OH bonds, because the isomer shift correlates not only with the d^n configuration of the iron center but also with the metal−ligand distances.[63,86] The calculated quadrupole splitting and magnetic-hyperfine splitting for model I also match the experimental values to within the accepted uncertainty (∼0.5 mm/s for quadrupole splittings and ∼3 MHz for hyperfine splittings).[67] The magnitude of the anisotropy of the hyperfine tensor in the xy plane calculated for I ($|A_x − A_y| = 6.4$ MHz) is comparable to the experimental value ($|A_x − A_y| = 5.9$ MHz). The significant underestimation of ZFS parameters for high-spin ferryl complexes has been observed in prior work[87] and stems largely from the intrinsically poor ability of DFT calculations to correctly predict spin-state energetics for transition metal complexes.[88] As analyzed elsewhere,[89−91] the predominant contributor to the ZFS parameter of an $S = 2$ ferryl unit is the extremely low-lying triplet excited state. To reach quantitative agreement, one must resort to more advanced *ab initio* approaches.[92]

For the $C_{Cys,β}$−H-cleaving intermediate, we considered interaction of a triplet O_2 with a high-spin Fe(II) to yield three possible total spin states ($S = 1$, 2, and 3) for the adduct (Figure 7B and Figure S15). In addition, two different binding modes of O_2, end-on and side-on, were evaluated (Figure S15). The triplet side-on species was not located, because, in the course of the geometry optimization, the O_2 moiety was seen invariably to rearrange to the end-on mode, as found in an earlier computational study.[40] The calculated key structural parameters (Table 2) are in reasonable agreement with those reported in earlier work,[40,41,93] although different computational procedures were employed there. The estimated marginal energy gaps between different spin states definitely fall within the computational uncertainty of DFT methods[88] and hence prevent further discrimination.[40,94] A similar situation was encountered in previous work examining possible structures of initial O_2 adducts in taurine:2-oxo-glutarate dioxygenase (TauD)[95] and homoprotocatechuate-2,3-dioxygenase (HPCD).[96] By contrast, spectroscopic parameters are usually much more sensitive to small geometric changes and thus provide a more reliable probe for the electronic structure.[96]

Table 2. Key Structural Parameters and Calculated Spin Hamiltonian Parameters for the Models of the Fe(III)-superoxo Intermediate

parameter	IV	V	VI	VII	VIII	exptl
spin	$S = 3$	$S = 3$	$S = 2$	$S = 2$	$S = 1$	
ΔE (kcal/mol)	0	0.5	1.3	0.2	2.1	
Fe−O	2.042	2.162	1.833	2.202	2.059	
Fe−O	3.197	2.186	2.930	2.156	2.892	
O−O	1.313	1.329	1.323	1.307	1.253	
δ (mm/s)	0.70	0.74	0.53	0.70	0.80	0.53
ΔE_Q (mm/s)	−0.63	0.62	1.12	0.66	3.50	1.02
η	0.1	0.3	0.8	0.3	0.2	
A (MHz)	−23.8	−24.0	−27.6	−31.7	−26.2	
	−24.8	−24.9	−29.4	−33.4	−26.8	
	−26.2	−26.4	−31.2	−35.4	−28.8	

Indeed, the computed isomer shift agrees with the experimental value only for model VI, whereas those for the other models are greater than the observed isomer shift by at least 0.17 mm/s (Table 2). In addition, the calculations on model VI also yield both a quadrupole-splitting parameter similar to the experimental value and a nearly isotropic hyperfine-coupling tensor as observed experimentally. Moreover, the computationally predicted A_{iso} value for model VI matches that determined experimentally to within the computational uncertainty (∼3 MHz).[67] Thus, model VI is consistent with all experimentally observed properties of the $C_{Cys,β}$−H-cleaving intermediate. As shown in the molecular orbital (MO) diagram of model VI (Figure S16), the upper valence region has six singly occupied MOs, of which five are Fe-3d based and the last one is O_2-π* centered. Because the electron residing in the O_2-π* MO has spin opposite to that on the Fe center, this intermediate is best formulated as a high-spin ferric center ($S_{Fe} = 5/2$) that is AF coupled to a superoxo radical ligand ($S_{SO} = 1/2$), in line with the electronic-structural description deduced by Mössbauer spectroscopy.

■ DISCUSSION

The Fe(III)-superoxo Intermediate and Its Role in β-Lactam Ring Closure. The first intermediate of the IPNS catalytic cycle, which accumulates after the addition of O_2 to the reactant complex, is the $C_{Cys,β}$−H-cleaving complex (C in Scheme 2). This intermediate accumulates to modest levels (∼14%) in the presence of selectively deuterated A[d_2-C]V substrate. When the reaction is carried out with unlabeled ACV substrate, the visible absorption features of this intermediate are barely discernible at short reactions times, and by the first reaction time accessible by conventional freeze-quench methodology (∼10 ms), the intermediate escapes under the detection limit of Mössbauer spectroscopy (<3%). The greater accumulation with the A[d_2-C]V substrate presumably results from a D-KIE on cleavage of the $C_{Cys,β}$−H bond and therefore provides direct evidence that the intermediate is the $C_{Cys,β}$−H-cleaving complex. The intermediate exhibits Mössbauer parameters consistent with a high-spin Fe(III)-superoxo species and broad absorption features centered at ∼630 and ∼500 nm.

Fe(III)-superoxo species have been proposed as early intermediates in virtually all MNH-Fe(II) enzymes.[20,21,24,25,45,46] However, they generally do not accumulate to levels allowing their identification or comprehensive spectroscopic and structural characterization. To our knowledge, only two MNH high-spin Fe(III)-superoxo complexes

have been spectroscopically characterized to date. Only one of these was detected in an enzyme, specifically in the H200N variant of the MNH-Fe(II) enzyme HPCD.[97] An Fe(III)-superoxo intermediate has been proposed as an intermediate in the native HPCD reaction cycle, but it is too reactive to be trapped. The combined use of a variant that perturbs the H-bonding network (H200N) and an analog with an electron-withdrawing group (4-nitrocatechol) led to accumulation of the cognate intermediate to a high level (80%). A combination of Mössbauer and parallel-mode EPR spectroscopies, coupled to DFT calculations, revealed that this complex is best described as having a high-spin Fe(III) site that is AF coupled to a superoxide radical anion, yielding an $S = 2$ electron-spin ground state.[97] The intermediate exhibits parallel-mode EPR features at $g = 8.17$, 8.8, and 11.6 and gives rise to both a Mössbauer quadrupole doublet in zero field ($\delta = 0.50$ mm/s and $\Delta E_Q = -0.33$ mm/s) and magnetically split Mössbauer spectra in externally applied magnetic fields. The Fe(III)-superoxo intermediate of H200N HPCD also exhibits an absorption band at 610 nm, close to the energy of the absorption feature at 630 nm observed for the IPNS Fe(III)-superoxo complex. The similarity of the spectroscopic properties of the IPNS intermediate to those of the complex in HPCD-H200N is additional support for the assignment of the IPNS complex as an Fe(III)-superoxo complex.

The second Fe(III)-superoxo complex is a recently reported inorganic model complex with the pentadentate ligand 2,6-bis-(((S)-2-(diphenylhydroxymethyl)-1-pyrrolidinyl)-methyl)-pyridine (H₂BDPP).[85] The reaction of [Fe(II)BDPP] with O₂ at −80 °C yielded the Fe(III)-superoxo complex, [Fe(III)BDPP-(O₂⁻•)], which has spectroscopic properties distinct from those of the cognate enzyme intermediates. [Fe(III)BDPP(O₂⁻•)] exhibits a magnetically split Mössbauer spectrum even in the absence of an applied field as a consequence of its unique electronic structure with two nearly degenerate ($\Delta E < 0.003$ cm⁻¹) electronic ground states. The total-electron-spin ground state of [Fe(III)BDPP(O₂⁻•)] was conclusively shown to be $S = 3$.[113]

The reactivity of the IPNS Fe(III)-superoxo intermediate is similar to that of the dinuclear Fe₂(III/III)-superoxo intermediate, termed G, of *myo*-inositol oxygenase (MIOX), despite the fact that the two enzymes differ in the nuclearities of their metallocofactors.[98,99] Like the IPNS Fe(III)-superoxo intermediate, G is formed by oxidative addition of O₂ to the Fe(II) site of the Fe₂(II/III) cofactor of MIOX, and it also cleaves an aliphatic C−H bond, the C1−H bond of the *myo*-inositol (cyclohexan-1,2,3,5/4,6-hexa-ol, MI) substrate. In the MIOX·MI complex, the C1-bonded oxygen of MI coordinates to the Fe(III) site of the cofactor,[100] just as the cysteinyl sulfur of ACV coordinates to the Fe(II) cofactor in IPNS.[38] Thus, for both enzymes, the C−H bond to be cleaved is activated by coordination (presumably with deprotonation) of an α-heteroatom.[45] The C−H(D) cleavage step effected by G of MIOX exhibits a moderate D-KIE, estimated to be 8−16.[98] The determination of the D-KIE in MIOX was complicated by the fact that (i) formation of G is reversible and (ii) it does not accumulate to appreciable levels with the unlabeled substrate and accumulates only to modest levels with the deuterium-labeled substrate.[98] The same challenges exist for determination of the D-KIE in the IPNS C−H-cleavage step. Nevertheless, a lower limit of 17 could be estimated by analysis of the ΔA_{515} kinetic traces from the reactions with unlabeled ACV and A[d_2-C]V.

Steps following C−H cleavage may also be similar in IPNS and MIOX. For IPNS, it is thought that the thioketyl radical intermediate undergoes an inner-sphere electron transfer to the Fe(III) center to form a hydroperoxo-Fe(II)/thioaldehyde complex (D → E), which is nucleophilically attacked by the deprotonated valine amide nitrogen to form the β lactam ring (E → F). Similarly, one of the proposed pathways for formation of MI in MIOX involves an inner-sphere electron transfer from the C1-ketyl radical intermediate to the Fe₂(III/III) cofactor to yield a hydroperoxo-Fe₂(II/III)-*myo*-inosose-1 intermediate (*myo*-inosose-1 is the C1-ketone of MI), which may undergo attack of the peroxide on the C1 carbonyl to initiate C1−C6 cleavage and generate the product, D-glucuronate.

The Fe(IV)-oxo Intermediate and Its Role in Thiazolidine Ring Formation. The second C−H-cleaving intermediate in the IPNS reaction is a high-spin Fe(IV) complex, presumably the high-spin ferryl species, F, in Scheme 2. It cleaves the $C_{Val,\beta}$−H-bond of the monocyclic β-lactam intermediate. The intermediate exhibits Mössbauer parameters typical of high-spin ferryl complexes trapped in other MNH-Fe(II) enzymes,[47,78,80−82,101,102] including an isomer shift of ~0.3 mm/s, a small negative quadrupole splitting parameter, and a positive axial ZFS parameter of ~10 cm⁻¹.[89] However, compared with other high-spin ferryl complexes, the anisotropy of the internal magnetic field in the *xy* plane (i.e., the plane perpendicular to the Fe=O bond) is greater, due to both a more pronounced rhombicity ($E/D = 0.09$) and a less axial hyperfine tensor ($|A_x| − |A_y| = 6$ MHz). The anisotropy of the hyperfine tensor features are well reproduced computationally. Another feature unique to the IPNS ferryl intermediate is its absorption bands, which are tentatively assigned to sulfur-to-iron charge transfer transitions.

The oxidation initiated by the ferryl intermediate of IPNS is reminiscent of that in the Fe(II)- and 2OG-dependent halogenases.[103] These enzymes use a *cis*-halo-ferryl intermediate to cleave an unactivated, aliphatic C−H bond by H• atom abstraction, yielding a presumptive *cis*-halo-Fe(III)−OH/substrate radical state. Attack of the substrate radical on the halide ligand coordinated *cis* to the hydroxide group yields the halogenated product and a coordinatively unsaturated Fe(II) site.[78,81,82,101] Likewise, in IPNS, the ferryl abstracts an unactivated H atom (F → G), and the resulting substrate radical attacks the *cis*-coordinated sulfur (G → H), yielding an Fe(II) site and the IPN product, which coordinates the Fe(II) center via its thioether sulfur.[39] For the halogenase SyrB2, it was shown that the position of the C−H bond to be cleaved relative to the ferryl moiety is the key factor resulting in the alternative outcome (halogenation rather than hydroxylation). Specifically, in SyrB2 the target C−H bond is positioned further away and in the equatorial plane, thereby decreasing C−H cleavage efficiency and disfavoring subsequent attack of the radical upon the hydroxo ligand.[82,104] The diminished C−H cleavage efficiency is evident in the decay rate constants of the ferryl, which are less by $10^2−10^3$ in the halogenase SyrB2 (0.07 s⁻¹ at 5 °C in the presence of the native, unlabeled substrate[82]) than in related hydroxylases [13 and ~300 s⁻¹ (both at 5 °C) for TauD and the prolyl-4-hydroxylase from *Paramecium bursaria Chlorella* virus I, each acting on protium-containing substrate[79,80]]. Consistent with this trend, decay of the ferryl complex in IPNS is slower ($k_{decay} = 6$ s⁻¹ at 5 °C with unlabeled ACV) than the corresponding C−H cleavage steps in the hydroxylases, but also significantly faster than C−H cleavage by the halogenases. Hydrogen abstraction by the ferryl in IPNS

exhibits a D-KIE of ≥ 30 (k_{decay} = 0.2 s^{-1} at 5 °C with AC[d_8-V]). We note that while it is possible to determine the decay rate constants with both isotopologs with good precision, the determination of the intrinsic D-KIE requires quantitatively accounting for potential unproductive reaction pathways,[44] which we have not yet investigated in IPNS.

Scheme 3. Comparison of the Thiazolidine and Oxazolidine Ring Formation Reactions Mediated by the Fe(IV)-oxo Intermediates of IPNS and Clavaminate Synthase (CAS)
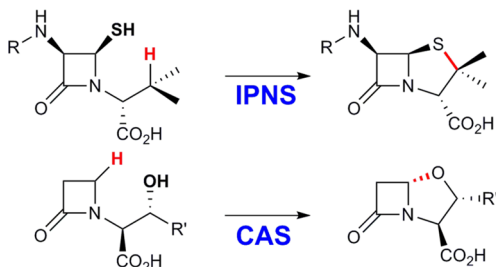
Thiazolidine ring formation in IPNS has evident analogy to formation of the oxazolidine ring in the biosynthesis of the important antibiotic, clavulanic acid, which is catalyzed by the enzyme clavaminate synthase (CAS) (Scheme 3).[105,106] CAS is an Fe(II)- and 2OG-dependent enzyme and catalyzes three distinct reactions (hydroxylation, desaturation, and formation of the oxazolidine ring) in the biosynthesis of clavulanic acid. The thiazolidine and oxazolidine-generating reactions are both 1,5-dehydrogenations and involve, formally, removal of hydrogen atoms from both an aliphatic carbon and the heteroatom (X = S, O) to be incorporated in the ring and formation of the new C−X bond. Both reactions are two-electron oxidations and are effected by ferryl intermediates, although the nature of the two-electron oxidation required for ferryl generation from the Fe(II) cofactor and O$_2$ is different in the two enzymes, [Fe(III)-superoxo-mediated β-lactam-ring formation in IPNS vs decarboxylation of the cosubstrate 2OG in CAS].

However, there is an important difference between the two reactions. The IPNS reaction involves attack of the substrate radical on an atom directly coordinated to the Fe center (sulfur from the β-lactam intermediate). In the case of CAS, there is no obvious open coordination site for the substrate to bind via the O atom that is incorporated into the oxazolidine ring. Indeed, magnetic circular dichroism (MCD) studies on CAS revealed an octahedral coordination environment of Fe in the CAS·Fe(II)·2OG complex, which consists of the "His$_2$(Asp/Glu) facial triad," the bidentate cosubstrate, 2OG, and a water molecule.[107] Addition of the substrate results in dissociation of the water ligand, thereby creating the necessary open coordination site for O$_2$ to bind.[107] Similar experiments on other Fe(II)/2OG enzymes[108] have shown that the generation of a coordinatively unsaturated Fe(II) primed for reaction with O$_2$ is a general feature of this enzyme family.[20] Thus, the substrate does *not* bind directly to the Fe center. An alternative mechanism has been proposed on the basis of a computational study for oxazolidine ring formation by CAS. Ring closure is initiated by abstraction of the hydrogen atom from the O−H group of the substrate by the ferryl.[109] Indeed, the X-ray crystal structure of the CAS·Fe(II)·2OG·proclavaminate complex reveals that the O atom that is incorporated into the thiazolidine ring is positioned only 4.2 Å from the Fe,[110] suggesting that O−H cleavage by the ferryl intermediate may

indeed be possible.[111] Ongoing efforts in our group are aimed at unraveling the mechanistic diversity of ferryl-mediated functionalization of unactivated carbon centers in greater depth.

■ ASSOCIATED CONTENT

ⓢ Supporting Information

The Supporting Information is available free of charge on the ACS Publications website at DOI: 10.1021/jacs.6b04065.

Materials, sequence of plasmid pIPNS, procedures for overexpression and purification of IPNS, procedure for synthesis of AC[d_8-V], LC/MS data demonstrating the IPNS-catalyzed conversion of ACV to IPN, ^{1}H NMR spectra of AC[d_8-V] and intermediates depicted in Scheme S1, raw SF-abs data from the reaction of O$_2$ with either IPNS·Fe(II)·ACV or IPNS·Fe(II)·A[d_2-C]V, comparison of SF-abs and FQ-Mössbauer features of the Fe(IV)-oxo intermediate and analysis of the Mössbauer spectra of this experiment, 4.2-K/variable-field Mössbauer spectra of the Fe(IV)-oxo intermediate and simulation thereof, 4.2-K/high-field Mössbauer spectra of a sample containing the Fe(III)-superoxo intermediate, depictions of model structures for the intermediates generated by DFT, orbital scheme of model VI of the Fe(III)-superoxo complex generated by DFT, relative quantities of the relevant species obtained from analysis of the 4.2-K/zero-field Mössbauer time courses (PDF)

■ AUTHOR INFORMATION

Corresponding Authors
*ckrebs@psu.edu
*jmb21@psu.edu
*shengfa.ye@cec.mpg.de
Author Contributions
$^\perp$E.T. and B.Z. both made contributions warranting primary authorship.
Notes
The authors declare no competing financial interest.

■ ACKNOWLEDGMENTS

■ REFERENCES

(1) Fleming, A. *Br. J. Exp. Pathol.* **1929**, *10*, 226.
(2) Abraham, E. P.; Gardner, A. D.; Chain, E.; Heatley, N. G.; Fletcher, C. M.; Jennings, M. A.; Florey, H. W. *Lancet* **1941**, *238*, 177.
(3) Chain, E.; Florey, H. W.; Gardner, A. D.; Heatley, N. G.; Jennings, M. A.; Orr-Ewing, J.; Sanders, A. G. *Lancet* **1940**, *236*, 226.
(4) Lyons, C. *J. Am. Med. Assoc.* **1943**, *123*, 1007.
(5) Tipper, D. J.; Strominger, Jl *Proc. Natl. Acad. Sci. U. S. A.* **1965**, *54*, 1133.
(6) Abraham, E. P.; Chain, E. *Nature* **1940**, *146*, 837.
(7) Livermore, D. M. *Clin. Microbiol. Rev.* **1995**, *8*, 557.

(8) Reading, C.; Cole, M. *Antimicrob. Agents Chemother.* **1977**, *11*, 852.

(9) Kershaw, N. J.; Caines, M. E. C.; Sleeman, M. C.; Schofield, C. J. *Chem. Commun.* **2005**, 4251.

(10) Arnstein, H. R. V.; Morris, D. *Biochem. J.* **1960**, *76*, 357.

(11) Loder, P. B.; Abraham, E. P. *Biochem. J.* **1971**, *123*, 471.

(12) Fawcett, P. A.; Abraham, E. P. *Methods Enzymol.* **1975**, *43*, 471.

(13) van Liempt, H.; von Döhren, H.; Kleinkauf, H. *J. Biol. Chem.* **1989**, *264*, 3680.

(14) Gutierrez, S.; Diez, B.; Montenegro, E.; Martin, J. F. *J. Bacteriol.* **1991**, *173*, 2354.

(15) Byford, M. F.; Baldwin, J. E.; Shiau, C. Y.; Schofield, C. J. *Chem. Rev.* **1997**, *97*, 2631.

(16) Samson, S. M.; Belagaje, R.; Blankenship, D. T.; Chapman, J. L.; Perry, D.; Skatrud, P. L.; VanFrank, R. M.; Abraham, E. P.; Baldwin, J. E.; Queener, S. W.; Ingolia, T. D. *Nature* **1985**, *318*, 191.

(17) Baldwin, J. E.; Abraham, E. P. *Nat. Prod. Rep.* **1988**, *5*, 129.

(18) Baldwin, J. E.; Bradley, M. *Chem. Rev.* **1990**, *90*, 1079.

(19) Baldwin, J. E.; Schofield, C. J. In *The Chemistry of β-Lactams*; Page, M. I., Ed.; Blackie: London, 1991; p 1.

(20) Solomon, E. I.; Brunold, T. C.; Davis, M. I.; Kemsley, J. N.; Lee, S. K.; Lehnert, N.; Neese, F.; Skulan, A. J.; Yang, Y.-S.; Zhou, J. *Chem. Rev.* **2000**, *100*, 235.

(21) Costas, M.; Mehn, M. P.; Jensen, M. P.; Que, L., Jr. *Chem. Rev.* **2004**, *104*, 939.

(22) Abu-Omar, M. M.; Loaiza, A.; Hontzeas, N. *Chem. Rev.* **2005**, *105*, 2227.

(23) Kovaleva, E. G.; Neibergall, M. B.; Chakrabarty, S.; Lipscomb, J. D. *Acc. Chem. Res.* **2007**, *40*, 475.

(24) Krebs, C.; Galonić Fujimori, D.; Walsh, C. T.; Bollinger, J. M., Jr. *Acc. Chem. Res.* **2007**, *40*, 484.

(25) Hausinger, R. P. *Crit. Rev. Biochem. Mol. Biol.* **2004**, *39*, 21.

(26) Fitzpatrick, P. F. *Biochemistry* **2003**, *42*, 14083.

(27) Gibson, D. T.; Parales, R. E. *Curr. Opin. Biotechnol.* **2000**, *11*, 236.

(28) Bugg, T. D. H.; Lin, G. *Chem. Commun.* **2001**, 941.

(29) Straganz, G. D.; Glieder, A.; Brecker, L.; Ribbons, D. W.; Steiner, W. *Biochem. J.* **2003**, *369*, 573.

(30) McCoy, J. G.; Bailey, L. J.; Bitto, E.; Bingman, C. A.; Aceti, D. J.; Fox, B. G.; Phillips, G. N. *Proc. Natl. Acad. Sci. U. S. A.* **2006**, *103*, 3084.

(31) Joseph, C. A.; Maroney, M. J. *Chem. Commun.* **2007**, 3338.

(32) Neidig, M. L.; Decker, A.; Choroba, O. W.; Huang, F.; Kavana, M.; Moran, G. R.; Spencer, J. B.; Solomon, E. I. *Proc. Natl. Acad. Sci. U. S. A.* **2006**, *103*, 12966.

(33) Pojer, F.; Kahlich, R.; Kammerer, B.; Li, S. M.; Heide, L. *J. Biol. Chem.* **2003**, *278*, 30661.

(34) Cicchillo, R. M.; Zhang, H. J.; Blodgett, J. A. V.; Whitteck, J. T.; Li, G. Y.; Nair, S. K.; van der Donk, W. A.; Metcalf, W. W. *Nature* **2009**, *459*, 871.

(35) Metcalf, W. W.; Griffin, B. M.; Cicchillo, R. M.; Gao, J. T.; Janga, S. C.; Cooke, H. A.; Circello, B. T.; Evans, B. S.; Martens-Habbena, W.; Stahl, D. A.; van der Donk, W. A. *Science* **2012**, *337*, 1104.

(36) Roach, P. L.; Clifton, I. J.; Fülöp, V.; Harlos, K.; Barton, G. J.; Hajdu, J.; Andersson, I.; Schofield, C. J.; Baldwin, J. E. *Nature* **1995**, *375*, 700.

(37) Roach, P. L.; Clifton, I. J.; Hensgens, C. M. H.; Shibata, N.; Long, A. J.; Strange, R. W.; Hasnain, S. S.; Schofield, C. J.; Baldwin, J. E.; Hajdu, J. *Eur. J. Biochem.* **1996**, *242*, 736.

(38) Roach, P. L.; Clifton, I. J.; Hensgens, C. M. H.; Shibata, N.; Schofield, C. J.; Hajdu, J.; Baldwin, J. E. *Nature* **1997**, *387*, 827.

(39) Burzlaff, N. I.; Rutledge, P. J.; Clifton, L. J.; Hensgens, C. M. H.; Pickford, M.; Adlington, R. M.; Roach, P. L.; Baldwin, J. E. *Nature* **1999**, *401*, 721.

(40) Lundberg, M.; Morokuma, K. *J. Phys. Chem. B* **2007**, *111*, 9380.

(41) Lundberg, M.; Siegbahn, P. E. M.; Morokuma, K. *Biochemistry* **2008**, *47*, 1031.

(42) Lundberg, M.; Kawatsu, T.; Vreven, T.; Frisch, M. J.; Morokuma, K. *J. Chem. Theory Comput.* **2009**, *5*, 222.

(43) Brown-Marshall, C. D.; Diebold, A. R.; Solomon, E. I. *Biochemistry* **2010**, *49*, 1176.

(44) Bollinger, J. M., Jr.; Krebs, C. *J. Inorg. Biochem.* **2006**, *100*, 586.

(45) Bollinger, J. M., Jr.; Krebs, C. *Curr. Opin. Chem. Biol.* **2007**, *11*, 151.

(46) van der Donk, W. A.; Krebs, C.; Bollinger, J. M., Jr. *Curr. Opin. Struct. Biol.* **2010**, *20*, 673.

(47) Price, J. C.; Barr, E. W.; Tirupati, B.; Bollinger, J. M., Jr.; Krebs, C. *Biochemistry* **2003**, *42*, 7497.

(48) Tamanaha, E. Ph.D. Thesis, The Pennsylvania State University, 2013.

(49) Münck, E. In *Physical Methods in Bioinorganic Chemistry*; Que, L., Jr., Ed.; University Science Books: Sausalito, CA, 2000; p 287.

(50) Becke, A. D. *J. Chem. Phys.* **1993**, *98*, 5648.

(51) Lee, C. T.; Yang, W. T.; Parr, R. G. *Phys. Rev. B: Condens. Matter Mater. Phys.* **1988**, *37*, 785.

(52) Grimme, S. *J. Comput. Chem.* **2006**, *27*, 1787.

(53) van Lenthe, E.; Baerends, E. J.; Snijders, J. G. *J. Chem. Phys.* **1993**, *99*, 4597.

(54) van Lenthe, E.; Baerends, E. J.; Snijders, J. G. *J. Chem. Phys.* **1994**, *101*, 9783.

(55) van Lenthe, E.; van Leeuwen, R.; Baerends, E. J.; Snijders, J. G. *Int. J. Quantum Chem.* **1996**, *57*, 281.

(56) van Wüllen, C. *J. Chem. Phys.* **1998**, *109*, 392.

(57) Pantazis, D. A.; Chen, X. Y.; Landis, C. R.; Neese, F. *J. Chem. Theory Comput.* **2008**, *4*, 908.

(58) Pantazis, D. A.; Neese, F. *J. Chem. Theory Comput.* **2009**, *5*, 2229.

(59) Neese, F.; Wennmohs, F.; Hansen, A.; Becker, U. *Chem. Phys.* **2009**, *356*, 98.

(60) Eichkorn, K.; Treutler, O.; Öhm, H.; Häser, M.; Ahlrichs, R. *Chem. Phys. Lett.* **1995**, *240*, 283.

(61) Klamt, A.; Schüürmann, G. *J. Chem. Soc., Perkin Trans. 2* **1993**, 799.

(62) Siegbahn, P. E. M. *JBIC, J. Biol. Inorg. Chem.* **2006**, *11*, 695.

(63) Neese, F. *Inorg. Chim. Acta* **2002**, *337*, 181.

(64) Schäfer, A.; Huber, C.; Ahlrichs, R. *J. Chem. Phys.* **1994**, *100*, 5829.

(65) Schäfer, A.; Horn, H.; Ahlrichs, R. *J. Chem. Phys.* **1992**, *97*, 2571.

(66) Römelt, M.; Ye, S. F.; Neese, F. *Inorg. Chem.* **2009**, *48*, 784.

(67) Sinnecker, S.; Slep, L. D.; Bill, E.; Neese, F. *Inorg. Chem.* **2005**, *44*, 2245.

(68) Neese, F. *J. Chem. Phys.* **2003**, *118*, 3939.

(69) Sinnecker, S.; Neese, F.; Noodleman, L.; Lubitz, W. *J. Am. Chem. Soc.* **2004**, *126*, 2613.

(70) Neese, F. *J. Chem. Phys.* **2007**, *127*, 164112.

(71) McWeeny, R.; Mizuno, Y. *Proc. R. Soc. London, Ser. A* **1961**, *259*, 554.

(72) Sinnecker, S.; Neese, F. *J. Phys. Chem. A* **2006**, *110*, 12267.

(73) Neese, F. *Wiley Interdiscip. Rev.: Comput. Mol. Sci.* **2012**, *2*, 73.

(74) An alternative solution with $k_1 = 7$ s^{-1} and $k_2 = 125$ s^{-1} is mathematically equivalent but predicts much less accumulation of the intermediate and would require a much greater molar absorptivity for it; Mössbauer-spectroscopic experiments and SF-abs-spectroscopic experiments with the $AC[d_8\text{-}V]$ isotopolog described below rule out this alternative solution.

(75) Gütlich, P.; Link, R.; Trautwein, A. X. *Mössbauer Spectroscopy and Transition Metal Chemistry*; Springer-Verlag: Berlin, 1978.

(76) Krebs, C.; Price, J. C.; Baldwin, J.; Saleh, L.; Green, M. T.; Bollinger, J. M., Jr. *Inorg. Chem.* **2005**, *44*, 742.

(77) Orville, A. M.; Chen, V. J.; Kriauciunas, A.; Harpel, M. R.; Fox, B. G.; Münck, E.; Lipscomb, J. D. *Biochemistry* **1992**, *31*, 4602.

(78) Matthews, M. L.; Krest, C. M.; Barr, E. W.; Vaillancourt, F. H.; Walsh, C. T.; Green, M. T.; Krebs, C.; Bollinger, J. M., Jr. *Biochemistry* **2009**, *48*, 4331.

(79) Price, J. C.; Barr, E. W.; Glass, T. E.; Krebs, C.; Bollinger, J. M., Jr. *J. Am. Chem. Soc.* **2003**, *125*, 13008.

(80) Hoffart, L. M.; Barr, E. W.; Guyer, R. B.; Bollinger, J. M., Jr.; Krebs, C. *Proc. Natl. Acad. Sci. U. S. A.* **2006**, *103*, 14738.

(81) Galonić, D. P.; Barr, E. W.; Walsh, C. T.; Bollinger, J. M., Jr.; Krebs, C. *Nat. Chem. Biol.* **2007**, *3*, 113.

(82) Matthews, M. L.; Neumann, C. S.; Miles, L. A.; Grove, T. L.; Booker, S. J.; Krebs, C.; Walsh, C. T.; Bollinger, J. M., Jr. *Proc. Natl. Acad. Sci. U. S. A.* **2009**, *106*, 17723.

(83) Baldwin, J. E.; Adlington, R. M.; Robinson, N. G.; Ting, H. H. *J. Chem. Soc., Chem. Commun.* **1986**, 409.

(84) Bencini, A.; Gatteschi, D. *EPR of Exchange Coupled Systems*; Springer-Verlag: Berlin, 1990.

(85) Chiang, C. W.; Kleespies, S. T.; Stout, H. D.; Meier, K. K.; Li, P. Y.; Bominaar, E. L.; Que, L., Jr.; Münck, E.; Lee, W. Z. *J. Am. Chem. Soc.* **2014**, *136*, 10846.

(86) Ye, S.; Bill, E.; Neese, F. *Inorg. Chem.* **2016**, *55*, 3468.

(87) Sinnecker, S.; Svensen, N.; Barr, E. W.; Ye, S.; Bollinger, J. M., Jr.; Neese, F.; Krebs, C. *J. Am. Chem. Soc.* **2007**, *129*, 6168.

(88) Ye, S.; Neese, F. *Inorg. Chem.* **2010**, *49*, 772.

(89) Neese, F. *J. Inorg. Biochem.* **2006**, *100*, 716.

(90) Bukowski, M. R.; Koehntop, K. D.; Stubna, A.; Bominaar, E. L.; Halfen, J. A.; Münck, E.; Nam, W.; Que, L., Jr. *Science* **2005**, *310*, 1000.

(91) Chanda, A.; Shan, X. P.; Chakrabarti, M.; Ellis, W. C.; Popescu, D. L.; Tiago de Oliveira, F.; Wang, D.; Que, L., Jr.; Collins, T. J.; Münck, E.; Bominaar, E. L. *Inorg. Chem.* **2008**, *47*, 3669.

(92) Ye, S.; Xue, G.; Krivokapic, I; Petrenko, T.; Bill, E.; Que, L., Jr.; Neese, F. *Chem. Sci.* **2015**, *6*, 2909.

(93) Brown, C. D.; Neidig, M. L.; Neibergall, M. B.; Lipscomb, J. D.; Solomon, E. I. *J. Am. Chem. Soc.* **2007**, *129*, 7427.

(94) Diebold, A. R.; Neidig, M. L.; Moran, G. R.; Straganz, G. D.; Solomon, E. I. *Biochemistry* **2010**, *49*, 6945.

(95) Ye, S. F.; Riplinger, C.; Hansen, A.; Krebs, C.; Bollinger, J. M., Jr.; Neese, F. *Chem. - Eur. J.* **2012**, *18*, 6555.

(96) Christian, G. J.; Ye, S. F.; Neese, F. *Chem. Sci.* **2012**, *3*, 1600.

(97) Mbughuni, M. M.; Chakrabarti, M.; Hayden, J. A.; Bominaar, E. L.; Hendrich, M. P.; Münck, E.; Lipscomb, J. D. *Proc. Natl. Acad. Sci. U. S. A.* **2010**, *107*, 16788.

(98) Xing, G.; Diao, Y.; Hoffart, L. M.; Barr, E. W.; Prabhu, K. S.; Arner, R. J.; Reddy, C. C.; Krebs, C.; Bollinger, J. M., Jr. *Proc. Natl. Acad. Sci. U. S. A.* **2006**, *103*, 6130.

(99) Bollinger, J. M., Jr.; Diao, Y.; Matthews, M. L.; Xing, G.; Krebs, C. *Dalton Trans.* **2009**, *6*, 905.

(100) Brown, P. M.; Caradoc-Davies, T. T.; Dickson, J. M. J.; Cooper, G. J. S.; Loomes, K. M.; Baker, E. N. *Proc. Natl. Acad. Sci. U. S. A.* **2006**, *103*, 15032.

(101) Galonić Fujimori, D.; Barr, E. W.; Matthews, M. L.; Koch, G. M.; Yonce, J. R.; Walsh, C. T.; Bollinger, J. M., Jr.; Krebs, C.; Riggs-Gelasco, P. J. *J. Am. Chem. Soc.* **2007**, *129*, 13408.

(102) Eser, B. E.; Barr, E. W.; Frantom, P. A.; Saleh, L.; Bollinger, J. M., Jr.; Krebs, C.; Fitzpatrick, P. F. *J. Am. Chem. Soc.* **2007**, *129*, 11334.

(103) Vaillancourt, F. H.; Yeh, E.; Vosburg, D. A.; Garneau-Tsodikova, S.; Walsh, C. T. *Chem. Rev.* **2006**, *106*, 3364.

(104) Martinie, R. J.; Livada, J.; Chang, W.-c.; Green, M. T.; Krebs, C.; Bollinger, J. M., Jr.; Silakov, A. *J. Am. Chem. Soc.* **2015**, *137*, 6912.

(105) Salowe, S. P.; Marsh, E. N. G.; Townsend, C. A. *Biochemistry* **1990**, *29*, 6499.

(106) Salowe, S. P.; Krol, W. J.; Iwata-Reuyl, D.; Townsend, C. A. *Biochemistry* **1991**, *30*, 2281.

(107) Pavel, E. G.; Zhou, J.; Busby, R. W.; Gunsior, M.; Townsend, C. A.; Solomon, E. I. *J. Am. Chem. Soc.* **1998**, *120*, 743.

(108) Neidig, M. L.; Brown, C. D.; Light, K. M.; Fujimori, D. G.; Nolan, E. M.; Price, J. C.; Barr, E. W.; Bollinger, J. M., Jr.; Krebs, C.; Walsh, C. T.; Solomon, E. I. *J. Am. Chem. Soc.* **2007**, *129*, 14224.

(109) Borowski, T.; de Marothy, S.; Broclawik, E.; Schofield, C. J.; Siegbahn, P. E. M. *Biochemistry* **2007**, *46*, 3682.

(110) Zhang, Z. H.; Ren, J. S.; Stammers, D. K.; Baldwin, J. E.; Harlos, K.; Schofield, C. J. *Nat. Struct. Biol.* **2000**, *7*, 127.

(111) Bollinger, J. M., Jr.; Chang, W.-c.; Matthews, M. L.; Martinie, R. J.; Boal, A. K.; Krebs, C. In *2-Oxoglutarate-Dependent Oxygenases*;

Hausinger, R. P., Schofield, C. J., Eds.; Royal Society of Chemistry: Cambridge, U.K., 2015; p 95.

(112) Hitchman, M. L. *Measurement of Dissolved Oxygen*; Wiley: New York, 1978; Vol. *49*.

(113) Stout, H. D.; Kleespies, S. T.; Chiang, C.-W.; Lee, W.-Z.; Que, L., Jr.; Münck, E.; Bominaar, E. L. *Inorg. Chem.* **2016**, *55*, 5215.